Title
The signaling phospholipid PIP3 creates a new interaction surface on the nuclear receptor SF-1

Journal
Proceedings of the National Academy of Sciences of the United States of America, 111(42)

ISSN
0027-8424

Authors
Blind, Raymond D
Sablin, Elena P
Kuchenbecker, Kristopher M
et al.

Publication Date
2014-10-21

DOI
10.1073/pnas.1416740111

Peer reviewed

The signaling phospholipid PIP_3 creates a new interaction surface on the nuclear receptor SF-1

Raymond D. Blind[a], Elena P. Sablin[b], Kristopher M. Kuchenbecker[b], Hsiu-Ju Chiu[c,d], Ashley M. Deacon[c,d], Debanu Das[c,d], Robert J. Fletterick[b,1], and Holly A. Ingraham[a,1]

Departments of [a]Cellular and Molecular Pharmacology and [b]Biochemistry and Biophysics, University of California, San Francisco, CA 94158; and [c]Joint Center for Structural Genomics and [d]Stanford Synchrotron Radiation Lightsource, SLAC National Accelerator Laboratory, Menlo Park, CA 94025

Contributed by Robert J. Fletterick, September 2, 2014 (sent for review June 27, 2014; reviewed by Eric Ortlund)

The signaling phosphatidylinositol lipids PI(4,5)P_2 (PIP_2) and PI(3,4,5)P_3 (PIP_3) bind nuclear receptor 5A family (NR5As), but their regulatory mechanisms remain unknown. Here, the crystal structures of human NR5A1 (steroidogenic factor-1, SF-1) ligand binding domain (LBD) bound to PIP_2 and PIP_3 show the lipid hydrophobic tails sequestered in the hormone pocket, as predicted. However, unlike classic nuclear receptor hormones, the phosphoinositide head groups are fully solvent-exposed and complete the LBD fold by organizing the receptor architecture at the hormone pocket entrance. The highest affinity phosphoinositide ligand PIP_3 stabilizes the coactivator binding groove and increases coactivator peptide recruitment. This receptor-ligand topology defines a previously unidentified regulatory protein-lipid surface on SF-1 with the phosphoinositide head group at its nexus and poised to interact with other proteins. This surface on SF-1 coincides with the predicted binding site of the corepressor DAX-1 (dosage-sensitive sex reversal, adrenal hypoplasia critical region on chromosome X), and importantly harbors missense mutations associated with human endocrine disorders. Our data provide the structural basis for this poorly understood cluster of human SF-1 mutations and demonstrates how signaling phosphoinositides function as regulatory ligands for NR5As.

transcription | nucleus | crystallography | ligand dependent | lipid transport

The existence of nuclear, nonmembrane pools of signaling phosphorylated derivatives of phosphatidylinositols or phosphoinositides (PIP_n) was reported over two decades ago (1–3). Consistent with these early reports, lipid-modifying enzymes responsible for phosphoinositide metabolism were also found in the nucleus (4–7); however, the function of PIP_n in this cellular compartment remains poorly defined. The nuclear receptors (NRs) steroidogenic factor 1 (SF-1, NR5A1) and liver receptor homolog 1 (LRH-1, NR5A2) bind phosphoinositides as well as other phospholipids in their large hydrophobic pockets (8–13). The ability of NR5As to interact with PIP_n is well-conserved with the *Caenorhabditis elegans* ortholog *nhr-25* able to bind both PIP_2 and PIP_3 (14). That phosphoinositides might serve as endogenous NR5A ligands is suggested by the fact that elevating cellular pools of PIP_3 increases SF-1 activity (15) and that impairing PIP_3 uptake decreases SF-1 activity (12). Further, when purified from mammalian cells, the phosphoinositide PIP_2 is found associated with SF-1 and can be modified by the lipid kinase, IPMK, as well as the lipid phosphatase, PTEN (13). Taken together, these data suggest that signaling phosphoinositides are biologically relevant ligands for SF-1.

Phosphoinositide ligands diverge chemically from classic NR hormones in that they contain a long, extended hydrophobic moiety and a prominent hydrophilic head group, which is inherently incompatible with the hydrophobic core of the NR5A ligand-binding pocket. Our previous structural analyses of SF-1 bound to phosphatidylcholine suggest that the acyl tails of phosphoinositides should be sequestered in the hydrophobic core and positioned to fill the hormone-binding pockets of SF-1 and LRH-1 (11). It remains to be determined how the acyl tails and the head groups of phosphoinositides might affect the stability and activity of the NR5A ligand-binding domain (LBD). To date, the only visualized phospholipid head groups in NR5As are those found in the bacterial phospholipids (bPLs), and long and medium chain phosphatidylcholines (PCs) (12, 16). Thus far, neither bPLs nor PCs complete the fold of SF-1 LBD. Indeed, in published ligand-bound SF-1 structures, critical surface loops in the vicinity of the pocket entrance remain poorly ordered. This region is functionally important because it harbors disease-associated mutations in SF-1 (17–19). We hypothesized that phosphoinositide ligands with their charged head groups might anchor this site to render SF-1 fully functional.

Here, the crystal structures of SF-1 bound to PIP_2 and PIP_3 were determined, and coactivator peptide-binding studies were performed to gain insights into how signaling phosphoinositides function as NR5A ligands. Based on our results, we suggest that PIP_2 and PIP_3 help organize dynamic loops in the LBD that form part of a previously unidentified regulatory surface on NR5As, similar in function to membrane-bound phosphoinositides.

Results

To establish which phosphoinositide species bind SF-1 LBD with the highest affinity, stoichiometric binding to Apo-SF-1 LBD was monitored in a native gel electrophoretic mobility-shift assay,

Significance

We previously reported that lipids PI(4,5)P_2 (PIP_2) and PI(3,4,5)P_3 (PIP_3) bind NR5A nuclear receptors to regulate their activity. Here, the crystal structures of PIP_2 and PIP_3 bound to NR5A1 (SF-1) define a new interaction surface that is organized by the solvent-exposed PIP_n headgroups. We find that stabilization by the PIP_3 ligand propagates a signal that increases coactivator recruitment to SF-1, consistent with our earlier work showing that PIP_3 increases SF-1 activity. This newly created surface harbors a cluster of human mutations that lead to endocrine disorders, thus explaining how these puzzling mutations cripple SF-1 activity. We propose that this new surface acts as a PIP_3-regulated interface between SF-1 and coregulatory proteins, analogous to the function of membrane-bound phosphoinositides.

Author contributions: R.D.B., E.P.S., R.J.F., and H.A.I. designed research; R.D.B., E.P.S., K.M.K., H.-J.C., A.M.D., and D.D. performed research; R.D.B. contributed new reagents/analytic tools; R.D.B., E.P.S., A.M.D., D.D., and R.J.F. analyzed data; and R.D.B., E.P.S., R.J.F., and H.A.I. wrote the paper.

Reviewers included: E.O., Emory University.

The authors declare no conflict of interest.

Freely available online through the PNAS open access option.

Data deposition: The atomic coordinates and structure factors have been deposited in the Protein Data Bank, www.pdb.org [PDB ID codes 4QJR (SF-1/PIP3) and 4QK4 (SF-1/PIP2)].

[1]To whom correspondence may be addressed. Email: robert.fletterick@ucsf.edu or holly.ingraham@ucsf.edu.

This article contains supporting information online at www.pnas.org/lookup/suppl/doi:10.1073/pnas.1416740111/-/DCSupplemental.

and the apparent K_d was determined for a series of related phosphoinositides. The resulting values suggest that 3- and 5-phosphates, but not the 4-phosphate, are critical coordination points for binding SF-1 LBD. Indeed, among all dioleyl (18:1) PIP_n ligands tested, $PI(3,4,5)P_3$ and $PI(3,5)P_2$ displayed the lowest K_d values of 80 ± 12 nM and 90 ± 12 nM, respectively (Fig. 1*A* and Table S1). In comparison, affinity of RJW100 (20), a derivative of the synthetic NR5A ligand GSK8470 (21), was notably worse than $PI(3,4,5)P_3$ with an apparent K_d of 1,200 ± 270 nM, as determined here by electrophoretic mobility-shift in native gels. We also noted that DLPC, a short-chained exogenous phosphatidylcholine LRH-1 ligand (16, 22), binds SF-1 poorly. In conjunction with these binding assays, differential scanning fluorimetry (DSF) was used to assess the stabilizing effects of different phospholipid ligands.

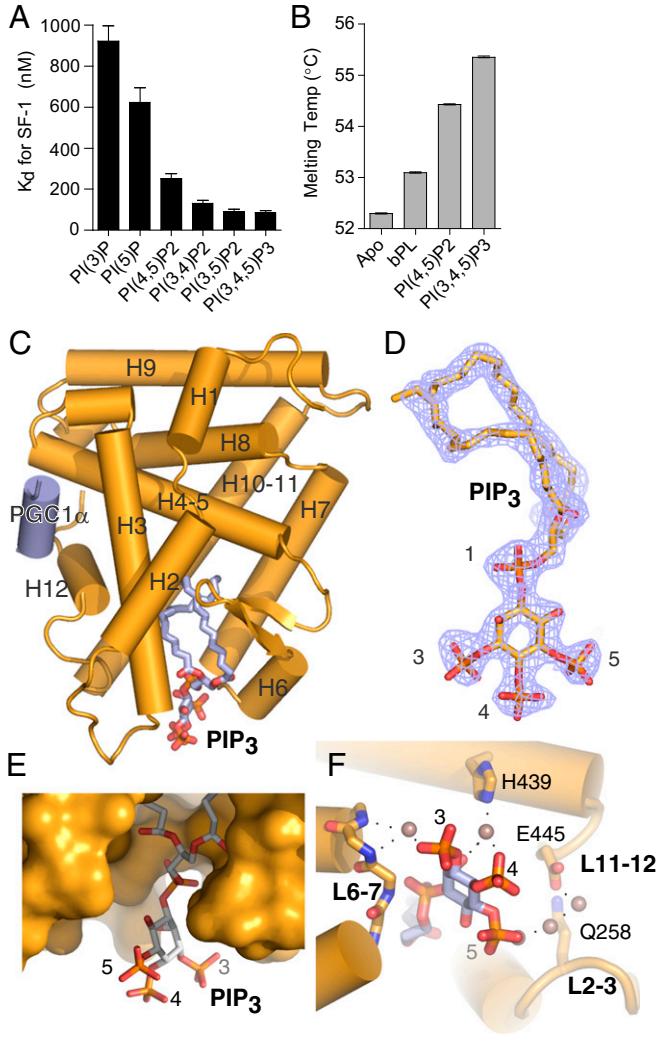

Fig. 1. Water coordination of the exposed head group in the SF-1/PIP_3 structure. (*A*) Apparent dissociation constants of indicated phosphoinositide lipids binding to the apo-SF-1 LBD. (*B*) Apparent melting temperatures of SF-1 LBD in the apo- (unliganded) state, complexed with copurifying bacterial phospholipid (bPL) PIP_2 or PIP_3 as determined by DSF. (*C*) Crystal structure of SF-1 LBD bound to PIP_3, PGC-1α coregulator peptide in blue, PIP_3 lipid as represented as sticks in all panels. (*D*) The final electron density map after model building and refinement ($2F_O - F_C$ contoured at 1.0 σ) demonstrating unambiguous assignment of PIP_3 acyl chains and head group stereochemistry. (*E*) Surface representation of SF-1, demonstrating exposure of PIP_3 head group to solvent. (*F*) Water (indicated as copper spheres)-mediated coordination of PIP_3 phosphate groups with indicated SF-1 amino acids in Loops L2-3, L6-7, and L11-12.

The melting temperatures of different ligand-bound states of SF-1 LBD showed the greatest stabilization with PIP_2 and PIP_3 phosphoinositides compared with the unliganded (apo) or bacterial phospholipid (bPL) bound receptor (Fig. 1*B*); bacterial phospholipids are present in NR5As from the bacterial expression system used to produce these proteins.

The structure of SF-1 LBD bound by dipalmitoyl (C16:0, C16:0) $PI(3,4,5)P_3$ (SF-1/PIP_3) was solved by the molecular replacement method using Protein Data Bank (PDB) entry 1YOW as the search model (11) and refined to 2.40 Å with R_{free}/R_{cryst} values of 23/19% (Table S2). The structure was deposited with the PDB ID code 4QJR. SF-1/PIP_3 (Fig. 1*C*) adopts the classic NR LBD fold consisting of 12 α-helices distributed in three layers with an extended helix H2 forming an additional fourth LBD layer. Similar to all other NR5A LBD structures, helix H12 assumes an active conformation, facilitating binding of PGC-1α coactivator peptide (Fig. 1*C*, blue cylinder).

The difference Fourier ($F_o - F_c$) electron density map for the SF-1 protein allowed unambiguous modeling of all elements of the dipalmitoyl (C16:0, C16:0) PIP_3 ligand (Fig. 1*D*) including the acyl chains, the bridging phosphate group at the tail-to-head junction, and the head group in a 1D-myo configuration (Fig. S1). As expected, the bridging phosphate group of PIP_3 is coordinated and makes contacts with conserved SF-1 residues G341, Y436, and K440 (Fig. S2). Although the acyl chains of PIP_3 are shielded from the solvent in the hydrophobic hormone-binding pocket, the head group of receptor-bound PIP_3 is fully exposed to the solvent (Fig. 1*E*); this unique feature sets SF-1/PIP_3 apart from other protein/PIP_n structures (23–25).

Protein loops never before visualized in other published ligand-bound SF-1 LBD structures are unusually well-ordered in the SF-1/PIP_3 structure (Fig. S3). Because these loops are not stabilized by any direct crystal contacts, we attribute this enhanced order in the SF-1/PIP_3 structure to the presence of a highly charged solvated PIP_3 head group that forms an extensive network of water-mediated interactions with the protein at the hormone pocket entrance. Stabilizing contacts involve residues in loops L2-3 (R255, D257, Q258), L6-7 (S342, L343), the C-terminal portion of H11 (H439), and the following loop L11-12 (N444, E445) (Fig. 1*F*); these data confirm our earlier findings that mutating H439 (H439D) decreases PIP_3 binding to SF-1 and diminishes SF-1 activity (12).

Due to stabilizing contacts with PIP_3, the loop between helices H2 and H3 (L2-3) is imaged, to our knowledge, for the first time with a clear conformation (Fig. 2 *A* and *B*). Water molecules organized by PIP_3 stabilize side chains of R255, D257, and Q258 in L2-3, which interact directly with residues N444 and E445 in L11-12 at the base of the activation function (AF)-2 helix H12. This network of stabilizing interactions configures helix H12 for optimal interactions with transcriptional coregulators (Fig. 2*C*). Loss-of-function heterozygous human *NR5A1* mutations R255L, R255C, and D257N present in L2-3 are associated with human diseases, including adrenal insufficiency (17), premature ovarian failure (18), and male infertility (19). The SF-1/PIP_3 structure reveals that both of these conserved residues, R255 and D257, interact with each other and form an anchoring cluster that organizes the protein–lipid surface at the entrance of the hormone pocket (Fig. 2*C*). Taken together, these data explain how *NR5A1* mutations in L2-3 cripple receptor activity (12), revealing the molecular basis of associated endocrine and reproductive disorders.

Our previous work suggests that SF-1 bound to PIP_3 is active whereas SF-1 bound to PIP_2 is less active (13). To compare these different phosphoinositide-bound states, the SF-1/$PI(4,5)P_2$ structure (SF-1/PIP_2) was solved by molecular replacement, using PDB ID code 1YOW as the search model, and compared with the SF-1/PIP_3 structure (Table S2). The structure was deposited with the PDB ID code 4QK4. Superposition of the SF-1 LBD in PIP_3- and PIP_2-bound states shows that these two structures are nearly identical (Fig. 3 *A* and *B*) (rms is 0.2 Å for 256 Cα atoms).

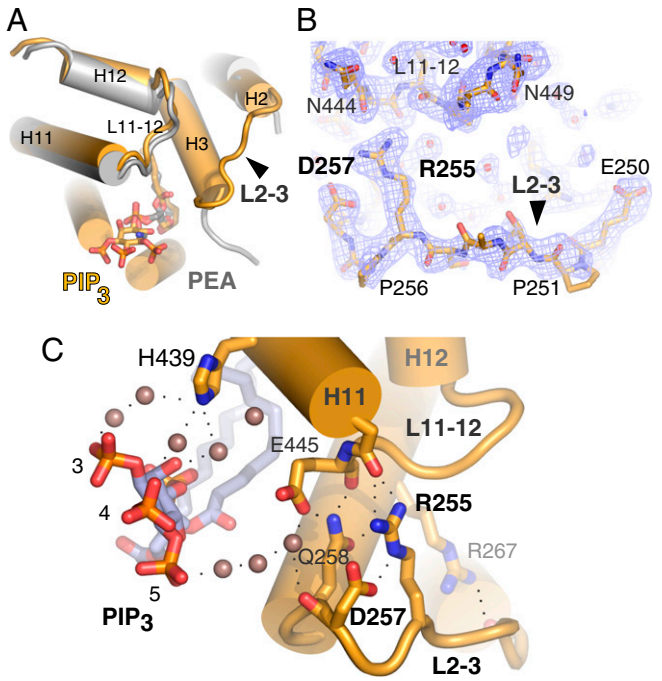

Fig. 2. PIP_3-mediated order in SF-1 loops reveals mechanism of R255 loss of function in human patients. (*A*) Current SF-1/PIP_3 structure (gold) superposed with the structure of SF-1 bound by bacterial phosphatidyl-ethanolamine (gray, PDB ID code 1ZDT) (46); arrow indicates newly ordered loop between helix 2 and helix 3 (L2-3). (*B*) Electron density map ($2F_O - F_C$ contoured at 1.0 σ) and stick representation of SF-1; arrow indicates newly ordered L2-3, with important residues labeled. (*C*) Water molecules (copper spheres) mediate stabilizing contacts between PIP_3 and human receptor residues R255, D257, N444, and E445. R267 stabilizes loop L2-3 at its base.

The lack of significant conformational differences between the two states could be explained by the dominant stabilizing effect of PGC1-α peptide used as a cocrystallization factor. Whereas the acyl chains of each bound ligand follow similar paths, the head group of PIP_2 is flipped relative to PIP_3 (Fig. 3*B* and Fig. S4), positioning the 5-phosphate group of PIP_2 within hydrogen bond distance from the critical H439 residue (Fig. 3*C*). These alternate conformations of the PIP_2 and PIP_3 head groups are reminiscent of the flipped orientations of the 5-phosphate of $PI(4,5)P_2$ and the 3-phosphate of $PI(3,4)P_2$ observed in the corresponding structures of the alpha-tocopherol transport protein, TTPα (24); the functional implications of these observations are unclear. The flipped orientation of the head group in the SF/PIP_2 structure might be favored by the electrostatic interaction between the 5-phosphate of PIP_2 and H439 residue (Fig. 3*C*); notably, this orientation of the head group mimics the configuration of the phosphate groups in the $PI(3,4)P_2$ that binds to SF-1 with high affinity (Table S1). Other than the flipped orientation of PIP_2 and PIP_3 head groups, all other features identified in the SF-1/PIP_2 and SF-1/PIP_3 structures were similar.

To further evaluate potential differences between SF-1/PIP_2 and SF-1/PIP_3 ligand-bound states, direct binding interactions between the SF-1 LBD and coactivator PGC1-α peptide were determined by surface plasmon resonance (SPR). This method was used to ask how different ligands bound to SF-1 affect the affinity of the PGC1-α peptide and is standardly used as a readout of ligand-dependent NR activation. Consistent with our observations showing the stabilizing effect of PIP_3 (Fig. 1*B*), SPR analyses show that PIP_3 induces a small, but significant, increase in SF-1 affinity for PGC-1α peptide at the AF2 site (Fig. 3*D* and Fig. S5).

The published crystal structure of mLRH-1 complexed with corepressor mDax-1 in its dimeric state shows that the second mDax-1 LBD is positioned at the NR5A hormone pocket entrance (26). Superposition of SF-1/PIP_3 and LRH-1/Dax-1 structures confirms that the PIP_3 head group and the second mDax-1 LBD are mutually exclusive as they occupy the same space (Fig. 4). In this regard, LRH-1 and SF-1 share high sequence and 3D-structural homology at this site. Thus, when SF-1 is bound by PIP_3, the exposed lipid–protein surface at the pocket entrance is expected to prevent the proposed repression by the Dax-1 dimer (27).

Taken together, our data demonstrate that PIP_3 is not merely a structural component of SF-1. Rather, this high-affinity phospholipid stabilizes dynamic regions at the pocket entrance, thus acting as a regulatory ligand to enhance receptor functionality through a novel protein–lipid interface. These findings, coupled with our previous work linking phosphoinositide signaling to SF-1 activity, begin to demonstrate how PIPs regulate NR5As.

Discussion

Here, structural and biochemical data show that PIP_3 functions as high-affinity, stabilizing ligand for SF-1. PIP_3 fills the hormone-binding pocket, organizes the flexible loops at the pocket entrance, and importantly is positioned with its electrostatic head group fully exposed (Fig. 5 *A* and *B*). We posit that the solvent-exposed phosphate groups of PIP_3 together with the stabilized surface

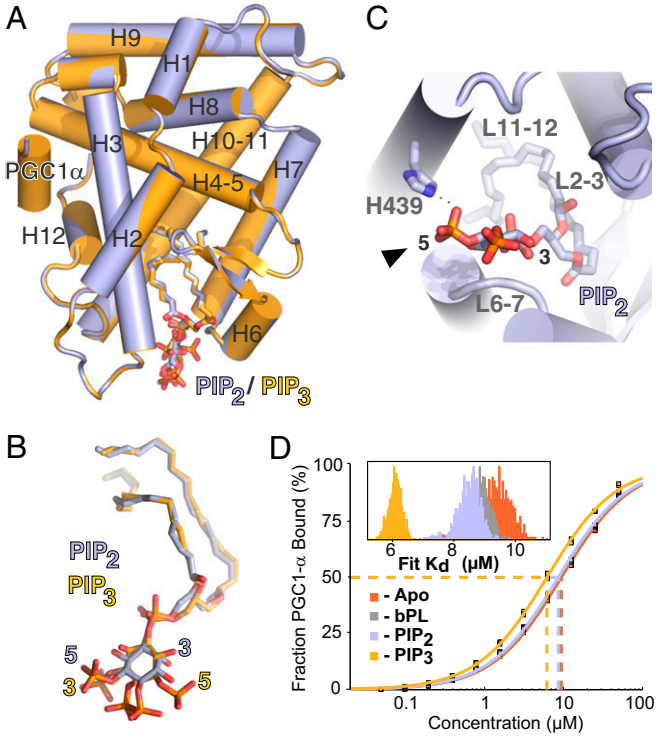

Fig. 3. SF-1/PIP_2 structure with helix 12 in the fully activated conformation. (*A*) Crystal structure of SF-1/PIP_2 (blue) superposed with SF-1/PIP_3 (gold). PGC-1α coregulator peptides are labeled and lipids are represented as sticks in all panels. (*B*) Superposition of PIP_2 and PIP_3 ligands bound to SF-1 and depicted as sticks. (*C*) Alternative view of SF-1/PIP_2, demonstrating exposure of PIP_2 head group to solvent and orientation of 5-phosphate. (*D*) Direct binding assays for four states of SF-1: bound to PIP_3, PIP_2, bPL or Apo. Relative K_d for PGC1-α peptide ±2 σ with histograms of fit K_d for four states shown in *Inset*. Mean and SD are calculated across all fits with Z-scores of SF-1/PIP3 versus Apo = 4.62, bPL = 4.99, and PIP2 = 4.43 (Z-statistic > 3.0 is highly significant). Binding curves with increasing concentrations of peptide are shown with dashed line indicating concentration at 50% bound ligand.

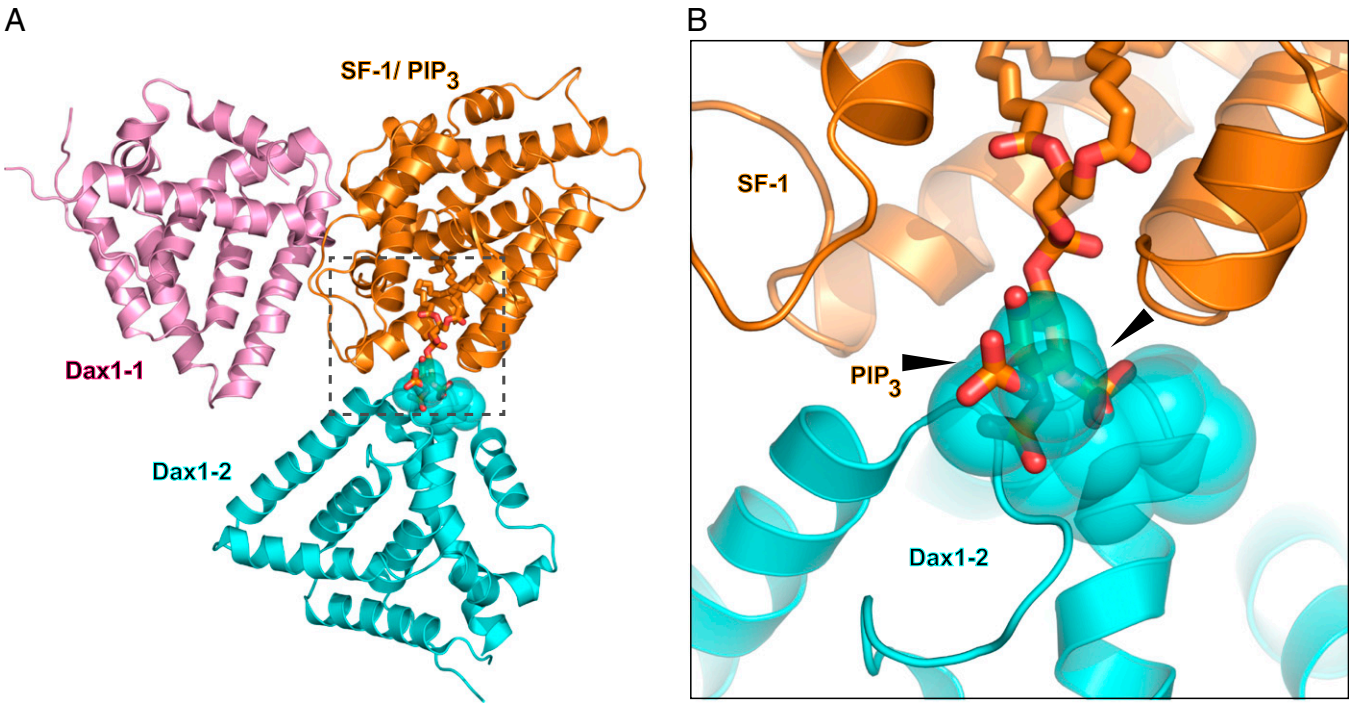

Fig. 4. PIP_3 interferes with Dax-1 corepressor interaction in simulations. (*A*) Schematic simulation of Dax1 monomer 1 (Dax1-1, pink) and monomer 2 (Dax1-2, cyan) interaction with SF-1/PIP_3 (gold), based on the LRH-1/Dax-1 crystal structure (PDB ID code 3F5C; rmsd = 0.91 Å over 237 Cα atoms). Dax1-1 interacts with the AF2 of SF-1 as expected whereas Dax1-2 interacts with a new surface on SF-1, which coincides with the PIP_3 head group. (*B*) Magnified view of the dashed box in *A*, demonstrating the steric clash between the PIP_3 head group and the Dax1-2 corepressor; arrowheads indicate points of collision. Side chains of Dax1-2 amino acids D283, Q284, and Q397 are represented as translucent cyan spheres, highlighting the coincidence.

loops function as an important regulatory site, forming a new molecular docking surface. This mechanism is analogous to the bridging functions of soluble inositols (28) or to membrane-bound PIP_3 in mediating protein–lipid interactions at the plasma membrane. Candidate binding partners that could dock to this nuclear protein–lipid complex might include the large group of nuclear proteins shown to bind directly to phosphoinositol phosphate head groups (29) or to contain pleckstrin-homology (PH)-domains (30, 31). Indeed, the phosphoinositide-dependent kinase-1 (PDK1) PH domain can be docked onto the SF-1/PIP_3 structure and can interface with the PIP_3 head group without any steric clashes at the solvent accessible surfaces (Fig. 5*C*). The inositol lipid kinase IPMK, previously shown to phosphorylate PIP_2 bound to SF-1, can also be docked onto the SF-1/PIP_2 structure without significant steric interference (32).

The functional significance of the opposing or "flipped" orientations of the PIP_2 and PIP_3 head groups in the SF-1 LBD structures presented here remains unclear. However, it is intriguing to note that the head groups of two phosphoinositides, $PI(3,4)P_2$ and $PI(4,5)P_2$, are also flipped in crystal structures of the TTPα lipid transport protein. Given that each position on the inositol head group has unique stereochemistry (33), one might imagine that the flipped orientations of the exposed PIP_2 and PIP_3 head groups differentially recruit stereo-specific coregulators. This hypothesis is consistent with our previous data showing that, at least on a subset of SF-1 target genes, PIP_3 but not PIP_2 is required for maximal SF-1 activity (13, 15).

The new lipid–protein surface created by the SF-1/PIP_n complex might also promote intramolecular domain interactions that have been observed in full-length structures of the PPARγ/RXRα heterodimer (34) and the HNF4α homodimer (35) and that are proposed to form a signaling nexus that controls NR function. An important prediction to emerge from our data is that effective drug targeting of NR5As must extend beyond the receptor hydrophobic pocket. Our findings suggest that a critical regulatory site for NR5As includes the entrance to the hormone-binding pocket. The 3D structures of full-length SF-1 receptor in various phosphoinositide-bound states should help to define the functional role of this novel lipid–protein surface and might offer new strategies for developing efficient NR5A1 drugs.

Similar to phospholipid transport proteins (PLTPs) (25, 36), NR5As bury the hydrophobic tails of phosphoinositides, making the phospholipids compatible with an aqueous environment (Fig. 5*D*). The SF-1 LBD could technically be classified as a PLTP, based on its ability to exchange phospholipids between membrane systems in vitro (7, 25). However, in the few available structures of PLTPs, the phosphoinositide head groups are not accessible to solvent (24, 25, 37). In stark contrast, our SF-1/PIP_n structures establish that the PIP_n head groups have unrestricted solvent accessibility, thus allowing lipid-modifying enzymes, such as IPMK and the lipid phosphatase PTEN to act on these exposed head groups (13). When considered as a PLTP that shuttles phospholipids within the nucleus, NR5As expand on that function by directly integrating lipid-signaling information into a transcriptional output (Fig. 5*D*). Whether or not SF-1 acts a sensor to detect the cellular phospholipid milieu in a living cell remains to be determined. Equally intriguing is whether phosphoinositides can be loaded into SF-1 by facilitated exchange with PLTPs or by direct extraction from intracellular membranes. Clearly, it will be of great interest to determine how signaling phosphoinositides are loaded into, and decoded by, NR5As to regulate gene expression.

Materials and Methods

Protein Expression and Purification. The LBD of human SF-1 (hSF-1) was purified to homogeneity as described for mouse SF-1 LBD (12). A Cys-lite version (C247S, C412S) of human SF-1 LBD was used for all crystallography. Briefly, hSF-1 LBD constructs in vector pBH4 spanning amino acids 218–461 were expressed in BL21 *Escherichia coli*, purified, and complexed with PIP_2 and

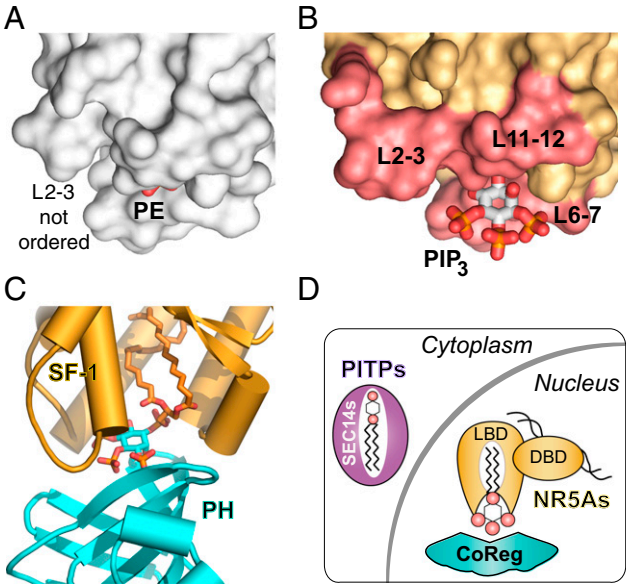

Fig. 5. PIP_3 induces a novel protein/lipid interaction surface. (*A*) Surface representation of bacterial phosphatidylethanol bound to human SF-1 LBD with the region of the disordered H2-3 indicated. (*B*) Same view as in *A*, but now PIP_3 is bound to SF-1, demonstrating ordered L2-3 and additional charges presented by the PIP_3 head group. (*C*) Docking simulation of the PH domain of PDK1 (cyan) interacting with SF-1/ PIP_3 (gold), showing possible complementarity between these two independent crystal structures. The head group (cyan) is from the PDK1 structure whereas the bridging phosphate and acyl chains are from the SF-1/PIP_3 structure. (*D*) Similar to other lipid transport proteins, SF-1 is able to resolve the conflict between the acyl chains of PIP_n and an aqueous environment. Formation of a new interaction surface used for recruiting regulatory proteins is possible when high-affinity phosphatidylinositol ligands bind SF-1.

PIP_3 purchased from Cayman. PIP_2 is PI(4,5)P_2 (1,2-dipalmitoyl-sn-glycero 3-phospho-(1′-myo-inositol-4′,5′-bisphosphate, ammonium salt) and PIP_3 is PI(3,4,5)P_3 (1,2-dipalmitoyl-sn-glycero 3-phospho-(1′-myo-inositol-3′,4′,5′-trisphosphate, sodium salt), and both are fully saturated C16:0 C16:0. Exogenous PIP_2 or PIP_3 was added to generate SF-1/phosphoinositide complexes, as previously described (13). Protein–phosphoinositide complexes were purified away from free phosphoinositides and bPL-bound SF-1 ligand-binding domain by Mono Q chromatography on an AKTA FPLC system (GE Biosciences) and concentrated for crystallization trials (15 mg/mL). A 3:1 molar excess of a peptide representing the human PGC1α cofactor (139-EEPSLLKKLLLAPA-152) was added to hSF-1/PIP_2 or hSF-1/PIP_3 complexes (15 mg/mL) in the presence of 10 μM PIP_2 or PIP_3, respectively.

Crystallization and Crystallographic Analyses of hSF-1 LBD/PIP_2 and /PIP_3. Both hSF-1/PIP_2:PGC1α and hSF-1/PIP_3:PGC1α complexes were crystallized by the vapor diffusion method, using a Mosquito (TTP Labtech), with reservoir solutions containing, respectively, 6% (vol/vol) PEG 8000, 0.2 M $Mg(OAc)_2$, and 20% (vol/vol) ethylene glycol for SF-1/PIP_2 or 10% PEG 8000, 25 mM $Mg(OAc)_2$, and 30% (vol/vol) glycerol for PIP_3-SF-1. Crystals were flash-frozen in liquid nitrogen. Native data were collected at the Stanford Synchrotron Radiation Lightsource (SSRL, SLAC National Accelerator Laboratory), at 100 K, using the MicroMax-002+ Microfocus X-ray generator (Rigaku) at a wavelength of 1.54 Å for SF-1/PIP_2 using a MarMosaic 325 CCD detector and beamline BL11-1 at a wavelength of 1.0 Å using a PILATUS 6M Pixel Array Detector for SF-1/PIP_3 and the BLU-ICE data collection environment (38). Data were integrated and scaled using programs XDS and XSCALE (39) to 2.81 Å resolution for PIP_2-SF-1 or MOSFLM (39) and SCALA (40), implemented in the CCP4 Program Suite (41), to 2.40 Å resolution for SF-1/PIP_3, and structure factor amplitudes were calculated using TRUNCATE (42). Both crystals were of the same space group $P4_12_12$ with cell dimensions of a = b = 75.0 Å, c = 138.6 Å (SF-1/PIP_2) and a = b = 74.9 Å, c = 139.6 Å (SF-1/PIP_3), respectively. Both crystals contained one ligand-bound SF-1 complex in the asymmetric unit. The structures of both complexes were determined by the molecular replacement method using PHASER (43) as implemented in PHENIX (44), with a search model derived from the atomic coordinates for hSF-1 (PDB ID code 1YOW) (11), with bound bacterial phospholipid and regulatory peptide omitted from the search model. Initial electron-density maps were calculated from the phases of the search model. Subsequent rounds of model building and refinement were performed using the PHENIX (44) and COOT (45) programs, respectively. At later stages, both structures were checked using simulated annealing composite omit maps. All figures illustrating structural data were generated using the PyMOL molecular graphics system (Schrödinger).

DSF Stability Assays. Protein thermo-stability in the presence and absence of tested phospholipids was assessed using the DSF method using the MxPro3005P qRT-PCR Detection System (Stratagene) in 96-well format. Binding of Sypro-Orange dye (Invitrogen) was monitored with a FAM filter for fluorescence excitation (492 nm) and a ROX filter for fluorescence emission (610 nm). The DSF spectra for purified wild-type hSF-1 LBD complexed with bacterial phospholipids PIP_2 or PIP_3 (10 μM) were recorded using a screening buffer (Tris-buffered saline) with added Sypro-Orange dye (1/2,000 dilution). Sample mixtures (final volume 50 μL) were heated gradually from 25 °C to 96 °C, at the rate of 2 °C/min, and the corresponding fluorescence was recorded after every 1 °C increase. The melting temperature (Tm) for each sample was deduced using the KaleidaGraph program (Synergy) from the first derivative of the corresponding denaturation curve generated by the MxPro QPCR software (Stratagene). Data represent at least three independent replicates.

Surface Plasmon Resonance Coactivator Peptide-Binding Assays. SPR analysis of human SF-1 LBD complexed with bPL, PIP_2, or PIP_3 was carried out on a Biacore T100 to measure the interaction between SF-1/phospholipid complexes and coregulator peptide. Matrix-free surfaces were prepared by injection of Neutravidin (Invitrogen) across a planar saccharide monolayer with covalently coupled biotin (BP chips; Xantec Bioanalytics) at 15 °C in 20 mM Hepes (pH 8.0), 150 mM NaCl. Fifteen-point concentration series were prepared by serial dilutions spanning 0.700–200 nM for human SF-1. Association and dissociation times were selected to ensure equilibrium and complete dissociation. All data were processed and analyzed in Matlab. Isotherms were fit to the Hill equation: fractional occupancy = $(c/(c + K_{1/2}))\hat{}n_H$, where c is the SF-1 concentration, $K_{1/2}$ is the SF-1 concentration producing half occupancy, and n_H is the Hill coefficient. Error in $K_{1/2}$ and n_H was determined by a bootstrap method with replacement: after scaling of n equilibrium responses for each peptide, a random set of n data points was selected with the possibility of selecting the same data point multiple times. After 1,000 iterations, the 100 best-fit parameters (sum of squared errors) were used to find mean values and SD. Parameters for $t_{1/2}$ were fit from the following equations: $R = R_o\ e\hat{}(-t \times k_{off})$ and $t_{1/2} = \ln(2)/k_{off}$, where R = response units. Data represent at least three independent replicates.

Native Gel K_d Determinations. Apparent dissociation constants of indicated SF-1 ligands were determined on apo-hSF-1 LBD by a previously described native gel shift assay to monitor equilibrium binding (13). Wild-type apo-hSF-1 LBD was generated by a dilution-washout procedure, as follows. Human SF-1 LBD was first loaded with PIP_3 and separated from any remaining bacterial phospholipid-bound SF-1 by ion exchange chromatography (Mono Q). The single SF-1/PIP_3 peak was diluted 2× with Mono Q buffer A and reloaded onto a Mono Q and washed with 1.0 L of 20 mM Hepes (8.0), 1 mM EDTA, and 2 mM CHAPS at 2 mL/min to washout PIP_3 from SF-1 LBD by dilution. The buffer was then changed into 20 mM Hepes (8.0), 1 mM EDTA to remove the CHAPS detergent, and the apo-SF-1 LBD was eluted as a single peak at 11 mS/cm conductivity, allowing complete separation from any SF-1 species still retaining PIP_3 phospholipid, which elutes as a single peak at 30 mS/cm conductivity due to the extra charge supplied by the PIP_3 head group phosphates.

All phosphoinositides used to determine apparent K_d were purchased from Avanti Polar lipids and were 1,2-dioleoyl-sn-glycero (C18:1, C18:1). Each phosphoinositide species was resuspended to 1 mg/mL in water, sonicated for 5 min on high power in a Branson Bioruptor bath sonicator, and then serially diluted and stored under nitrogen at 4 °C. Immediately before use, phosphoinositides were sonicated again. Two microliters of serially diluted phosphoinositide were added to binding reactions of 25 μL total volume, containing 1 μM final concentration of apo-hSF-1 LBD in 20 mM Hepes (8.0), 1 mM EDTA, and 10 mM ammonium acetate in 200 μL of polypropylene PCR strip tubes. Binding reactions were incubated at 37 °C for 1 h in a PCR thermocycler with a heated reaction cover, and the reaction was mixed with 3 μL of native loading buffer [40% (vol/vol) glycerol, 0.005% Ponceau S] and run on a 4–16% polyacrylamide Bis-Tris NativePage gel (Invitrogen). After fixation and silver staining (Bio-Rad), gels were scanned, the phosphoinositide-shifted band were quantitated using NIH Image, and apparent K_d was

determined by nonlinear curve fit to a single-site binding model in GraphPad Prism. RJW100 was resuspended in DMSO with the final DMSO concentration in the binding reactions to be 2.5% of the total reaction volume. Data represent at least three independent replicates.

ACKNOWLEDGMENTS. We thank Ms. T. Ruban for technical assistance in this project and Dr. C. Benod for initial guidance on the DSF, as well as members of the H.A.I. and R.J.F. laboratories and Dr. M. A. Elsliger for discussion and review of the manuscript. We also thank members of the Joint Center for Structural Genomics (JCSG) High Throughput Structural Biology pipeline for contributions to this work. Support for this project included Grants R01DK072246 and R01DK099722 (to H.A.I.), National Institute of General Medical Sciences (NIGMS)-Institutional Research and Academic Career Development Awards Fellowship K12GM081266 and Grant 1K01CA172957 (to R.D.B.), Grant R01DK078075, Department of Defense Grant W81XWH-12-1-0396, and Protein Structure Initiative (PSI) Grant U01 GM094614 as part of the PSI-Biology Partnership for Stem Cell Biology (to R.J.F.). The JCSG is supported by National Institutes of Health (NIH), NIGMS, Protein Structure Initiative U54 GM094586. This work was carried out as part of the PSI-Biology Partnership for Stem Cell Biology. Use of the Stanford Synchrotron Radiation Lightsource (SSRL), SLAC National Accelerator Laboratory, is supported by the US Department of Energy (DOE), Office of Science, Office of Basic Energy Sciences under Contract DE-AC02-76SF00515. The SSRL Structural Molecular Biology Program is supported by the DOE Office of Biological and Environmental Research and by the NIH through Grant P41 GM103393.

1. Cocco L, et al. (1987) Synthesis of polyphosphoinositides in nuclei of Friend cells. Evidence for polyphosphoinositide metabolism inside the nucleus which changes with cell differentiation. *Biochem J* 248(3):765–770.
2. Vann LR, Wooding FB, Irvine RF, Divecha N (1997) Metabolism and possible compartmentalization of inositol lipids in isolated rat-liver nuclei. *Biochem J* 327(Pt 2): 569–576.
3. Boronenkov IV, Loijens JC, Umeda M, Anderson RA (1998) Phosphoinositide signaling pathways in nuclei are associated with nuclear speckles containing pre-mRNA processing factors. *Mol Biol Cell* 9(12):3547–3560.
4. Martelli AM, et al. (1992) Nuclear localization and signalling activity of phosphoinositidase C beta in Swiss 3T3 cells. *Nature* 358(6383):242–245.
5. Divecha N, Banfić H, Irvine RF (1991) The polyphosphoinositide cycle exists in the nuclei of Swiss 3T3 cells under the control of a receptor (for IGF-I) in the plasma membrane, and stimulation of the cycle increases nuclear diacylglycerol and apparently induces translocation of protein kinase C to the nucleus. *EMBO J* 10(11): 3207–3214.
6. Shah ZH, et al. (2013) Nuclear phosphoinositides and their impact on nuclear functions. *FEBS J* 280(24):6295–6310.
7. Balla T (2013) Phosphoinositides: Tiny lipids with giant impact on cell regulation. *Physiol Rev* 93(3):1019–1137.
8. Ingraham HA, Redinbo MR (2005) Orphan nuclear receptors adopted by crystallography. *Curr Opin Struct Biol* 15(6):708–715.
9. Li Y, et al. (2005) Crystallographic identification and functional characterization of phospholipids as ligands for the orphan nuclear receptor steroidogenic factor-1. *Mol Cell* 17(4):491–502.
10. Ortlund EA, et al. (2005) Modulation of human nuclear receptor LRH-1 activity by phospholipids and SHP. *Nat Struct Mol Biol* 12(4):357–363.
11. Krylova IN, et al. (2005) Structural analyses reveal phosphatidyl inositols as ligands for the NR5 orphan receptors SF-1 and LRH-1. *Cell* 120(3):343–355.
12. Sablin EP, et al. (2009) Structure of SF-1 bound by different phospholipids: Evidence for regulatory ligands. *Mol Endocrinol* 23(1):25–34.
13. Blind RD, Suzawa M, Ingraham HA (2012) Direct modification and activation of a nuclear receptor-PIP_2 complex by the inositol lipid kinase IPMK. *Sci Signal* 5(229): ra44.
14. Mullaney BC, et al. (2010) Regulation of C. elegans fat uptake and storage by acyl-CoA synthase-3 is dependent on NR5A family nuclear hormone receptor nhr-25. *Cell Metab* 12(4):398–410.
15. Lin BC, et al. (2009) Stimulating the GPR30 estrogen receptor with a novel tamoxifen analogue activates SF-1 and promotes endometrial cell proliferation. *Cancer Res* 69(13):5415–5423.
16. Lee JM, et al. (2011) A nuclear-receptor-dependent phosphatidylcholine pathway with antidiabetic effects. *Nature* 474(7352):506–510.
17. Biason-Lauber A, Schoenle EJ (2000) Apparently normal ovarian differentiation in a prepubertal girl with transcriptionally inactive steroidogenic factor 1 (NR5A1/SF-1) and adrenocortical insufficiency. *Am J Hum Genet* 67(6):1563–1568.
18. Philibert P, et al. (2013) NR5A1 (SF-1) gene variants in a group of 26 young women with XX primary ovarian insufficiency. *Fertil Steril* 99(2):484–489.
19. Röpke A, et al. (2013) Comprehensive sequence analysis of the NR5A1 gene encoding steroidogenic factor 1 in a large group of infertile males. *Eur J Hum Genet* 21(9): 1012–1015.
20. Whitby RJ, et al. (2011) Small molecule agonists of the orphan nuclear receptors steroidogenic factor-1 (SF-1, NR5A1) and liver receptor homologue-1 (LRH-1, NR5A2). *J Med Chem* 54(7):2266–2281.
21. Whitby RJ, et al. (2006) Identification of small molecule agonists of the orphan nuclear receptors liver receptor homolog-1 and steroidogenic factor-1. *J Med Chem* 49(23):6652–6655.
22. Musille PM, et al. (2012) Antidiabetic phospholipid-nuclear receptor complex reveals the mechanism for phospholipid-driven gene regulation. *Nat Struct Mol Biol* 19(5): 532–537, S531-532.
23. de Saint-Jean M, et al. (2011) Osh4p exchanges sterols for phosphatidylinositol 4-phosphate between lipid bilayers. *J Cell Biol* 195(6):965–978.
24. Kono N, et al. (2013) Impaired α-TTP-PIPs interaction underlies familial vitamin E deficiency. *Science* 340(6136):1106–1110.
25. Schaaf G, et al. (2008) Functional anatomy of phospholipid binding and regulation of phosphoinositide homeostasis by proteins of the sec14 superfamily. *Mol Cell* 29(2): 191–206.
26. Sablin EP, et al. (2008) The structure of corepressor Dax-1 bound to its target nuclear receptor LRH-1. *Proc Natl Acad Sci USA* 105(47):18390–18395.
27. Iyer AK, Zhang YH, McCabe ER (2006) Dosage-sensitive sex reversal adrenal hypoplasia congenita critical region on the X chromosome, gene 1 (DAX1) (NR0B1) and small heterodimer partner (SHP) (NR0B2) form homodimers individually, as well as DAX1-SHP heterodimers. *Mol Endocrinol* 20(10):2326–2342.
28. Watson PJ, Fairall L, Santos GM, Schwabe JW (2012) Structure of HDAC3 bound to co-repressor and inositol tetraphosphate. *Nature* 481(7381):335–340.
29. Jungmichel S, et al. (2014) Specificity and commonality of the phosphoinositide-binding proteome analyzed by quantitative mass spectrometry. *Cell Reports* 6(3): 578–591.
30. Yu JW, et al. (2004) Genome-wide analysis of membrane targeting by S. cerevisiae pleckstrin homology domains. *Mol Cell* 13(5):677–688.
31. Lemmon MA (2004) Pleckstrin homology domains: Not just for phosphoinositides. *Biochem Soc Trans* 32(Pt 5):707–711.
32. Blind RD (2014) Disentangling biological signaling networks by dynamic coupling of signaling lipids to modifying enzymes. *Adv Biol Regul* 54:25–38.
33. Shears SB (2004) How versatile are inositol phosphate kinases? *Biochem J* 377(Pt 2): 265–280.
34. Chandra V, et al. (2008) Structure of the intact PPAR-gamma-RXR- nuclear receptor complex on DNA. *Nature* 456(7220):350–356.
35. Chandra V, et al. (2013) Multidomain integration in the structure of the HNF-4α nuclear receptor complex. *Nature* 495(7441):394–398.
36. Ren J, Schaaf G, Bankaitis VA, Ortlund EA, Pathak MC (2011) Crystallization and preliminary X-ray diffraction analysis of Sfh3, a member of the Sec14 protein superfamily. *Acta Crystallogr Sect F Struct Biol Cryst Commun* 67(Pt 10):1239–1243.
37. Tilley SJ, et al. (2004) Structure-function analysis of human [corrected] phosphatidylinositol transfer protein alpha bound to phosphatidylinositol. *Structure* 12(2): 317–326.
38. McPhillips TM, et al. (2002) Blu-Ice and the Distributed Control System: Software for data acquisition and instrument control at macromolecular crystallography beamlines. *J Synchrotron Radiat* 9(Pt 6):401–406.
39. Leslie AGW, Powell HR (2007) Processing diffraction data with Mosflm. *Evolving Methods for Macromolecular Crystallography: The Structural Path to the Understanding of the Mechanism of Action of Cbrn Agents.* Nato Science Series Series II: Mathematics, Physics, and Chemistry, eds Read RJ, Sussman J (Springer, Dordrecht, The Netherlands), Vol 245, pp 41–51.
40. Evans P (2006) Scaling and assessment of data quality. *Acta Crystallogr D Biol Crystallogr* 62(Pt 1):72–82.
41. Winn MD, et al. (2011) Overview of the CCP4 suite and current developments. *Acta Cryst* D67:235–242.
42. French S, Wilson K (1978) On the treatment of negative intensity observations. *Acta Crystallogr A* 34:517–525.
43. McCoy AJ, et al. (2007) Phaser crystallographic software. *J Appl Crystallogr* 40(4): 658–674.
44. Adams PD, et al. (2010) PHENIX: A comprehensive Python-based system for macromolecular structure solution. *Acta Crystallogr D Biol Crystallogr* 66(Pt 2):213–221.
45. Emsley P, Lohkamp B, Scott WG, Cowtan K (2010) Features and development of Coot. *Acta Crystallogr D Biol Crystallogr* 66(Pt 4):486–501.
46. Wang W, et al. (2005) The crystal structures of human steroidogenic factor-1 and liver receptor homologue-1. *Proc Natl Acad Sci USA* 102(21):7505–7510.